Integration of Microporosity Prediction in Durable and Robust Component Designs of Highly Loaded Aluminum Castings

M.Sc. **M. Weidt**, MAGMA Gießereitechnologie GmbH, Aachen, Germany
Prof. Dr.-Ing. **A**. **Bührig-Polaczek**, Foundry Institute, RWTH Aachen University

1. Abstract

Cyclically loaded cast aluminum components continue to be subjected to strong pressure to increase power density, particularly through increased specific loads or by weight reduction. To achieve these goals, it is necessary to fully exploit the material-specific performance potential. At the same time, robust manufacturing processes require precise knowledge of the main influencing variables linking process parameters, component design, and component performance. A closed simulation chain and the systematic use of virtual test plans (DoE) promise the targeted development of components and optimized and robust production. This paper presents in detail one of the main influencing variables in the simulation chain, the relationship between the existing local porosity and the resulting defect size. In an integrated approach, the obtained information will be used to predict the local fatigue strength and combined with the residual stress state to predict the fatigue performance for an aluminum cylinder head. By validation component tests it can be shown that only this integrated approach allows a satisfactory failure prediction under cyclic loading.

2. Motivation and Background

Combustion engines are subjected to static and cyclic loads during operation. In particular, the cyclic loads that can be borne depend not only on the alloy composition and local microstructure but also to a large extent on existing microstructural defects. During the solidification of aluminum castings, it is hardly possible under real production conditions to completely avoid a certain number of property-reducing defects such as intermetallic phases, inclusions, or micropores. Among these defects, micropores often represent by far the largest

local defect in the microstructure and therefore significantly determine the cyclic properties [1], [2].

The ongoing efforts to reduce the weight of internal combustion engines while at the same time increase power density are increasingly raising the requirements for full utilization of the material's strength potential.

Design decisions have a direct impact not only on the load distribution of the component but also on the local material properties and defect distributions. Faster solidification leads to a finer microstructure formation, which is usually associated with advantageous material properties. However, design decisions can also have a negative influence on the local solidification behavior and can increase the formation of porosity, as well as cause or intensify residual stress-related casting defects such as hot tearing and cold cracks. It is of great advantage to assess the consequences of decisions regarding cast part and casting process design while still in the planning stage. At this point, the virtual design of experiments (DOE) tool is available as part of the integrated casting process simulation. By systematically working through virtual experiments, safe process windows can be identified at the design stage of the casting. The complex interactions between component design, manufacturing conditions, and unavoidable fluctuations in manufacturing become manageable by a virtual DOE.

The results presented in this paper are based on the systematic analysis of microporosity in a cylinder head using computed tomography at the micrometer scale. The goal of this work is to develop a better understanding of the relationships between porosity, pore size, and pore morphology. With this information available, a methodology to predict the local cyclic fatigue performance should be realized. The extension includes the effect of microporosity in addition to the influence of microstructure; thus it significantly improves the correct representation of the local material behavior of castings compared to the standard approach where only the local dendrite arm spacing (DAS) is considered. Moreover, it is shown that the residual stress state of the casting is a significant contributor to the actual failure behavior.

3. Casting Process

In this paper, the results of a cylinder head, manufactured by NEMAK Linz, Austria, using the Rotacast® process [3], are presented. Here, the melt is transferred from the holding furnace to a tundish by an automated pouring ladle. The tundish then docks with the prepared mold from below. A 180° rotational movement around the longitudinal axis fills the mold uniformly and with low turbulence. The cylinder heads were cast using two alloys, AlSi7Cu0.5Mg and AlSi8Cu3. Both alloys are typical for internal combustion engine applications, were melted from grain refined ingots and modified by strontium addition before casting.

Samples were taken from the cylinder heads from three areas, each with different solidification rates: near the combustion chamber, in the tween deck, and the camshaft bearing. The objective was to cover a wide range of solidification conditions and the resulting microporosity.

4. Microcomputed Tomography and Data Preparation

The analysis of porosity distribution and pore shapes are based on 30 specimens, five specimens each (from five cylinder heads) in three positions and with two alloys. Sampling was carried out at the Department of General Mechanical Engineering at the University of Leoben, Austria. Computed tomographic analysis was performed by the Materials Center Leoben, Austria, using a GE nanotom m (XCT). Depending on the expected microstructure fineness, a spatial resolution of 3 µm voxel size (rapidly solidified samples) and 8 µm voxel size (slowly solidified samples) was used (voxel size = three-dimensional equivalent to a two-dimensional pixel). At the resolution of 3 µm and 8 µm, respectively, the scanned sample volume averages at about 144 and 477 mm^3 across all corresponding samples.

By setting a threshold value, each voxel was defined to be pore volume or dense metal. Digital image post-processing was then used to artificially increase the resolution of the resulting pore volumes. Adjacent pore volumes were "merged" and analyzed as one larger pore. The criterion for aggregation was based on the distance between two pores and their equivalent spherical diameters: If the smaller equivalent sphere diameter met or exceeded the pore spacing, the pores were combined. The analysis routine used for this purpose was developed by the Department of General Mechanical Engineering at the University of Leoben in Austria. Details of the XCT measurements and analyses, as well as the suitability of the XCT radiation source, the required spatial resolution, the required size of the scanned volume, and data processing techniques, are discussed elsewhere by Garb et al. [4].

Figure 1 shows a pore with its associated convex envelope. To characterize the size of each pore, the largest dimension of these envelopes was defined as the envelope diameter d_e. The maximum value within each sample is referred to below as the maximum envelope diameter $d_{e,max}$.

The measure of sphericity describes how far the quotient of volume to the surface area of a body deviates from that of a sphere. With the help of this quantity, the morphology of a pore can be characterized. Here, the sphericity must be within the values 1 "perfect sphere" and 0 "perfect deviation from a sphere". The sphericity of a pore is calculated using:

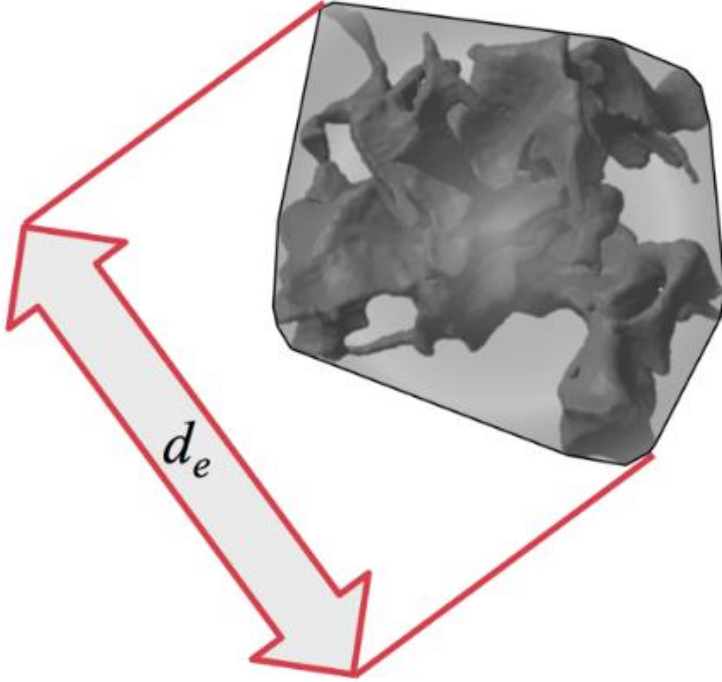$$\psi_i = \frac{\pi^{\frac{1}{3}}(6v_i)^{\frac{2}{3}}}{s_i}$$

(Equation 1)

Figure 1: Representation of the largest dimension of a convex pore envelope (d_e)

Here s_i and v_i are the surface area and volume of a single pore, respectively.

To describe the characteristic pore morphology within a sample, a volume-weighted mean sphericity ψ_{mean} is determined, also referred to as mean sphericity in the following. This parameter weights large pores, due to their volume, significantly stronger than small pores. In the conducted evaluations, this approach was shown to be very reliable with regard to the use of different resolutions in CT scanning. Also, it minimizes the influence of very small pores that lie at the resolution limit of the computer tomograph. These very small pores are the most error-prone ones and are negligible for lifetime prediction.

$$\psi_{mean} = \frac{\sum_N(v_i\psi_i)}{\sum_N v_i}$$

(Equation 2)

In this equation, *N* represents the total number of all pores within a sample.

5. Result of the Pore Analyses

Table 1 summarizes the minimum and maximum characteristic porosity parameters determined by the previously presented methods.

	Porosity, g_p (vol.-%)	Maximum envelope diameter, $d_{e,max}$ (µm)	Mean weighted sphericity, ψ_{mean}
Min	0.003	218	0.18
Max	0.392	3961	0.90

Table 1: List of minimum and maximum characteristic porosity values of all 30 evaluated samples

As can be seen from Table 1, there are significant differences between the measured values. The porosity varies from very low values of 0.003 vol % to moderate values of 0.392 vol %. Due to the non-standardized evaluation routine of the CT measurements as well as the post-processing of the data, no measurement error can be specified. Therefore the main focus lay on determining the pore size as robustly as possible.

Compared to the small variations in total porosity, significant differences occur for both the maximum envelope diameter $d_{e,max}$ (about 0.2 to 4 mm) and the characteristic pore morphology ψ_{mean} (0.18 to 0.90). This shows that the individual pores have significantly different shape characteristics within a narrow overall total range in porosity. A more precise understanding of the correlation between these variables is thus essential for quantitative statements about the material's application behavior.

Figure 2 shows exemplarily a sample of the alloy AlSi8Cu3 from the tween deck in 3D. The sample contains only 0.176% porosity but has a maximum diameter of the pore envelopes of 2.75 mm. The pores are highly tortuous, i.e. twisted and branched. Thus, a small absolute pore volume already leads to significant pore dimensions. A small amount of porosity can lead to defect sizes that are relevant for cyclic fatigue prediction.

Figure 3 shows the relationship between the maximum envelope diameter and porosity for the two investigated alloys. The trend is assumed to be linear in the first approximation and the scatter around the assumed linear relationship increases significantly with increasing porosity.

The presumed linear relationship between maximum envelope diameter and porosity is noteworthy in that all samples from both alloys follow the same trend despite being apart by about 2.5 wt % in copper and about 1 wt % in silicon as well as being extracted from three different positions with varying solidification rates.

The higher maximum porosity level exhibited by the AlSi8Cu3 alloy samples can be explained primarily by the increased copper content. Copper is known to destabilize the eutectic solidification front in cast aluminum alloys, causing the last solidifying zone to solidify in a spongy manner [6]. The resulting reduced permeability of the solidifying microstructure leads to earlier isolation of fluid regions, forming the potential for larger porosity volumes.
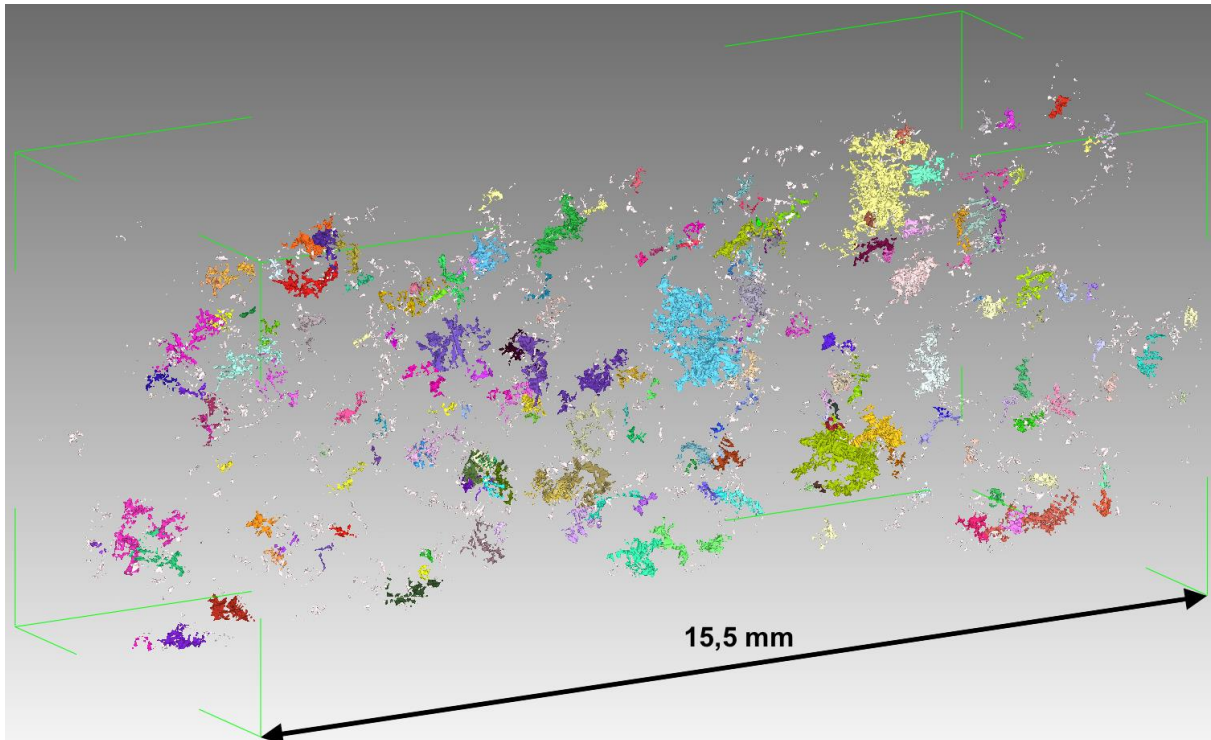

Figure 2: Three-dimensional representation of an XCT sample from the tween deck of an AlSi8Cu3 cylinder head. The porosity is 0.176 %, the maximum diameter of the pore envelope is $d_{e,max}$ 2.75 mm. The coloring of the individual pores is done randomly and serves only for better differentiation of the individual pores [5].

A sufficiently high local thermal gradient can in turn shorten the feeding paths of the sponge-like zone, compensating for the negative effects of the increased copper content on porosity. Moreover, copper in combination with strontium as a eutectic refining agent increases the size of eutectic cells [7]. This results in an enlargement of the liquid residual melt areas - and a higher porosity potential. Finally, an increased copper content increases the solidification interval, especially in the Terminal Freezing Range (TFR$_{85-95}$: temperature interval between the solid fraction of 85 % and 95 %). The Al$_2$Cu phase formed at the end of solidification exhibits a high volume contraction (about 8.4 vol %) upon solidification. The first factor reduces the feeding capacity of the alloy, the second factor increases the local feeding demand.

Another difference between the two alloys is the significantly higher iron content of the AlSi8Cu3 alloy, which is described in the literature as increasing porosity [8]. In both cases,

however, the alloys contain sufficient amounts of manganese to form the α-$Al_{15}(Fe,Mn)_3Si_2$ phase instead of β-Al_5FeSi. In contrast to the β-phase, the α-phase has an equiaxed topology, which makes it less detrimental to local feeding at the microstructure level and hardly increases the potential for pore formation [9].

Figure 4 plots the evolution of the mean sphericity ψ_{mean} against porosity. With increasing porosity, a continuous decrease of the mean sphericity can be observed. The presumed relationship was approximated with a fit function (see Figure 4). This function results in a theoretical sphericity limit of 0.08 for high porosities and of about 0.8 for a porosity value approaching zero. The samples of both investigated alloys follow the same trend.

Despite the differences presented between the two alloys, the same basic behavior exists concerning the relationship of pore size to porosity amount (see Fig. 3), it can be assumed that there is also no direct dependence for the pore shape on the chemical composition, the solidification rate, or the length of the mushy zone (see Fig. 4). Rather, the dendritic structure present at the end of solidification seems to dictate the available space for pore formation. At very low porosity contents, pores with high sphericity are observed. Round pores are the expected undisturbed shape to minimize the interfacial energy. The shape of small pores is largely determined by this factor, especially since their shape is only slightly affected by contact with the dendritic structure due to their small size. As more porosity is formed, the maximum pore envelope increases linearly (see Fig. 3). In relation to the pore volume, this leads to a disproportionate increase in the pore surface - compared to a sphere with the same volume. Figure 4 shows this in the form of decreasing mean sphericity with increasing porosity. This decrease in sphericity is due to increased growth restriction of the growing pores by the dendritic microstructure. The higher the existing amount of porosity, the more tortuous the largest pores become. Further analysis [10] has shown that this behavior is not necessarily the case, but is probably limited to melt of low gas content (in the case of aluminum casting alloys low hydrogen). In the case of the specimens presented in this work, pore formation can be assumed to occur very late in the solidification process. The dendritic microstructure thus has a strong impact on the development of the pore shape.
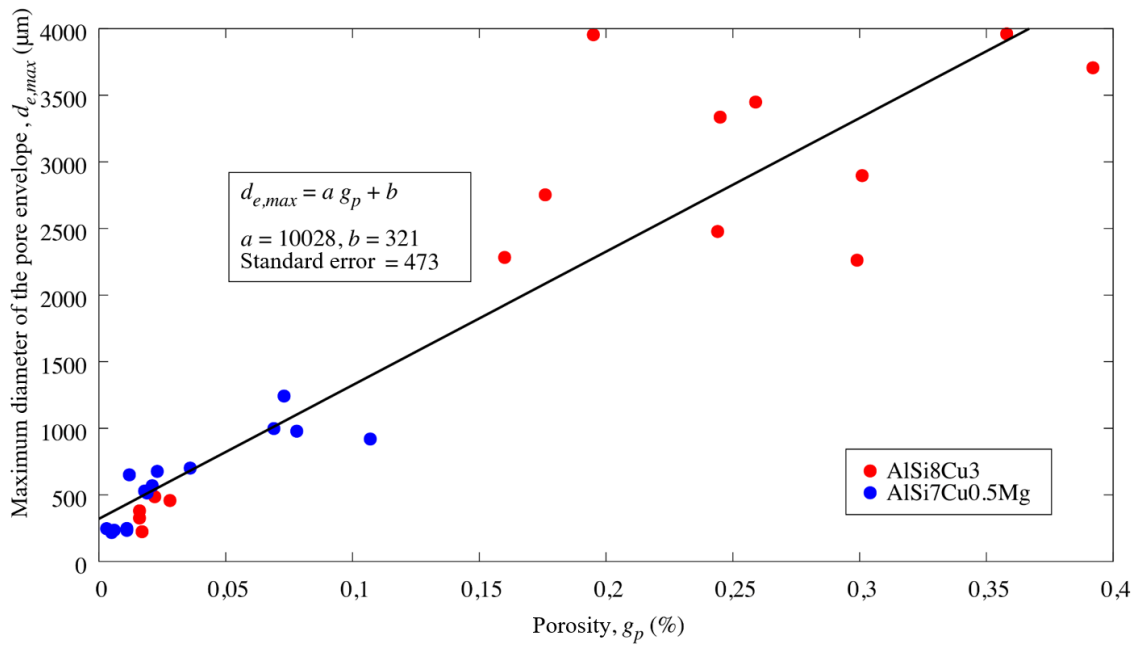
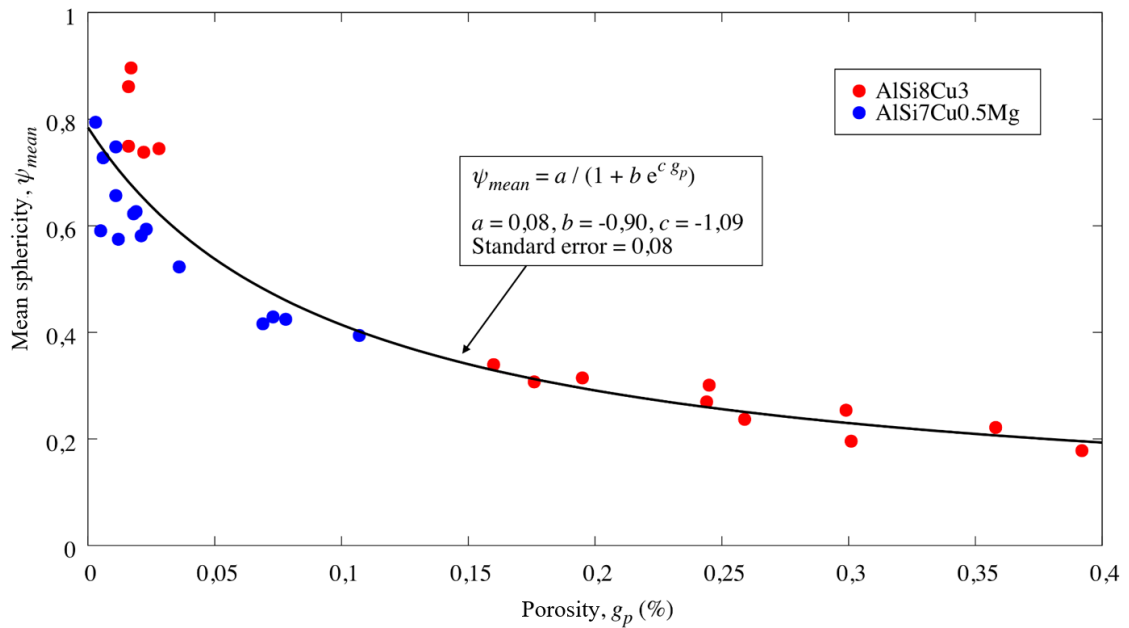Figure 3: Plot of maximum envelope diameter plotted against porosity [5].

Figure 4: Plot of volume-weighted mean sphericity versus porosity

6. Residual Stress Distribution after Heat Treatment

The casting process and heat treatment of aluminum castings can lead to significant residual stresses. Since these residual stresses can have both beneficial and detrimental effects on the

loads that can be borne when the component is used, they must be taken into account already during the component design. If disadvantageous stress conditions cannot be avoided due to the part design, sensible adjustments (geometry, quenching process after solution annealing) can already be made at this stage. For the AlSi7Cu0.5Mg cylinder head, the residual stresses were calculated based on its T6W heat treatment (water quenched) using MAGMASOFT® [A]. MAGMASOFT® can also be used to account for the stress redistributions resulting from cutting a sample from the cylinder head. The result is shown in Figure 5.

After heat treatment, significant residual stresses are present in the casting. With a Von Mises equivalent stress of more than 90 MPa in case of the T6W treatment, these must be taken into account in a fatigue simulation. The main cause of the high stresses is the different cooling rates during water quenching after solution heat treatment (T6W). The mechanical removal of the camshaft bearing samples for the validation tests from the heat-treated cylinder heads results in the redistribution of the residual stresses. This process involves cutting the specimen region clear from the overall cylinder head and then calculating a new mechanical equilibrium in the specimen. The result is a changed stress state with asymmetrical stress distribution in the notch area. The Von Mises stress reaches values of up to approx. 50 MPa, see Fig. 5.
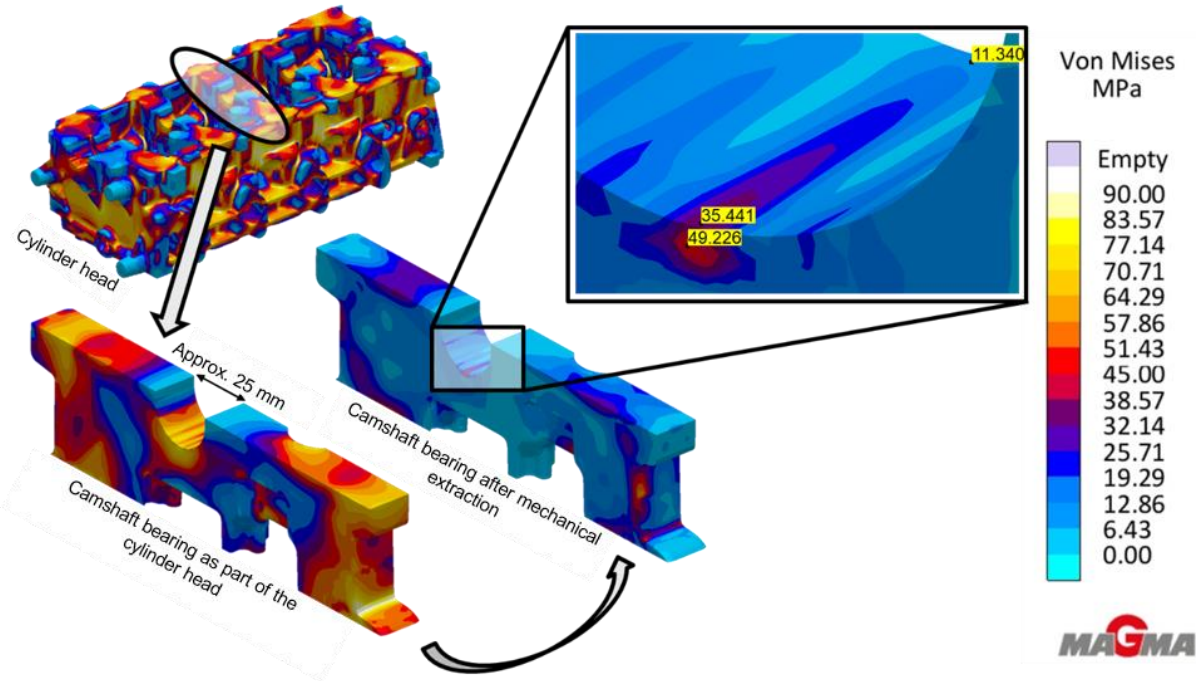

Figure 5: Representation of the simulated Von Mises equivalent stress after T6W heat-treatment of the entire cylinder head (top left), in the camshaft bearing as part of the cylinder head (bottom left) and after mechanical extraction of the camshaft bearing for the validation tests (center)

7. Estimation of Local Fatigue Strength Using the Example of the Camshaft Bearing

It is common practice to predict the local dendrite arm spacing (DAS) from the local solidification time. This in turn can be simply correlated with the tensile strength. In die casting the DAS, via the local cooling rate, is strongly controlled by the respective distance to the mold wall. As the distance from the mold surface increases, the DAS in the camshaft bearing increases. Simple correlations can therefore be used to predict the local tensile strength *(R_m)* using tensile tests for known values of the DAS. The tensile strength can be used for improved estimation of cyclic properties through established approaches. It becomes clear that this approach only takes into account the local solidification rate. Local changes in thermal gradient, alloy-specific solidification morphology, or microporosity do not affect the predicted fatigue properties. Thus, while this approach leads to improved component design compared to constant material properties, it does not account for local effects. Significant deviations between the expected and the observed failure behavior do remain.

By considering the local microporosity and thus the locally present defect size in terms of the maximum diameter of the pore envelopes, the above approach can be significantly extended. For the prediction of local microporosity, several different models are described in the literature. In this work, reference is made to the publication by Carlson et al. [11], which was used to predict the local amount of microporosity for the camshaft region of the cylinder head. Even though a very low porosity level prevails in most areas, significantly higher local microporosity levels are also evident, some of which exceed the investigated test space. Therefore, the predicted porosity level was limited to 0.5% by volume.

The defect size and microstructure characteristics allow the prediction of the local cyclic fatigue properties [12]. Figure 6 shows a comparison of the fatigue strength in tension-compression loading calculated by MAGMASOFT® in the center of the camshaft bearing. The classical approach considering only the DAS (left) shows the effect of the decreasing cooling rate from the die to the thermal center in the middle of the casting. Only by including the microporosity (right) are local effects taken into account, such as the reduction of microporosity near the sand core as well as the effect of a large thermal gradient.

To prove the suitability of the explained concept, the Institute for General Mechanical Engineering in Leoben, Austria, conducted validation tests for the camshaft bearing. Similarly, AVL List GmbH simulated the failure behavior using the FEMFAT software. All local mechanical properties used in FEMFAT, as well as the existing residual stresses, were transferred using the MAGMAlink module. Figure 7 summarizes again the newly developed

approach for predicting the actual failure behavior of an aluminum casting: The component behavior is predicted realistically only by including the locally present microporosity as well as the residual stresses from the casting and heat-treatment process.

Figure 8 shows the results of the validation tests with the camshaft bearing samples. The properties (tension-compression fatigue strength and residual stress state) were transferred to the FE mesh in the test condition. Without taking local material properties and residual stresses into account, a realistic prediction of the failure behavior is not possible.

If only residual stresses combined with homogeneous material properties are taken into account, the vibration resistance is overestimated (Fig. 8 yellow data series). The same is true if the DAS without residual stresses is considered (Fig. 8 green data series). Compared to the first case (yellow data series) the deviation between the real tests and the simulation is smaller. Only by considering both factors, i.e. the local residual stress state and the local property distribution, the observed cyclic component behavior can be satisfactorily predicted (Fig. 8 red data series).
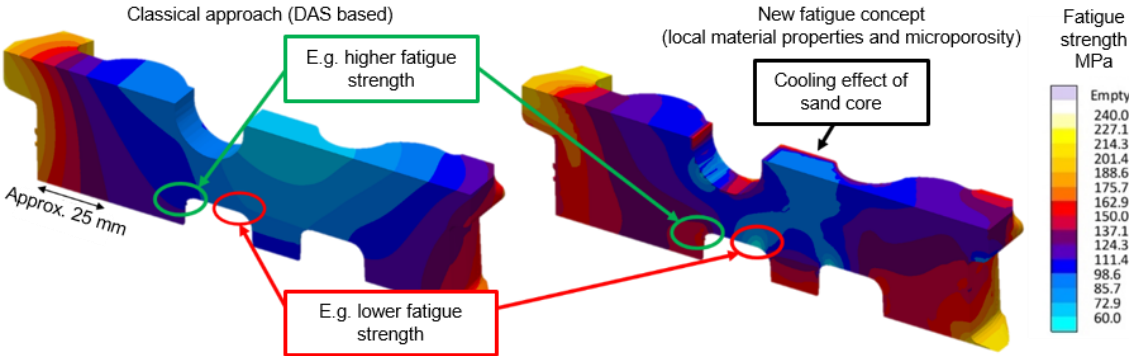

Figure 6: Plot of the tension-compressive fatigue strength in section through the center of the camshaft bearing using the "classical" approach, based on the local DAS (left), as well as based on the additionally included microporosity prediction and the derived defect size (right)
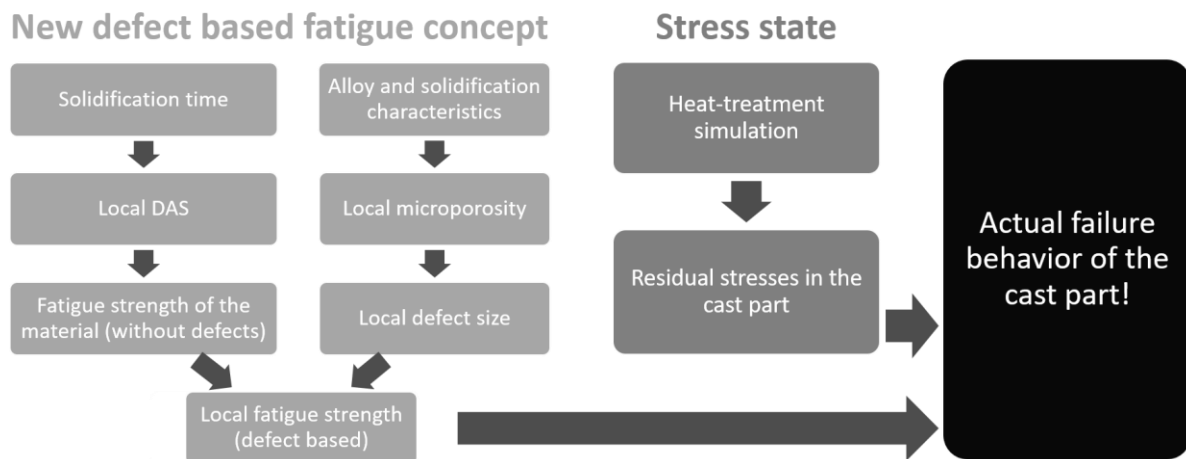
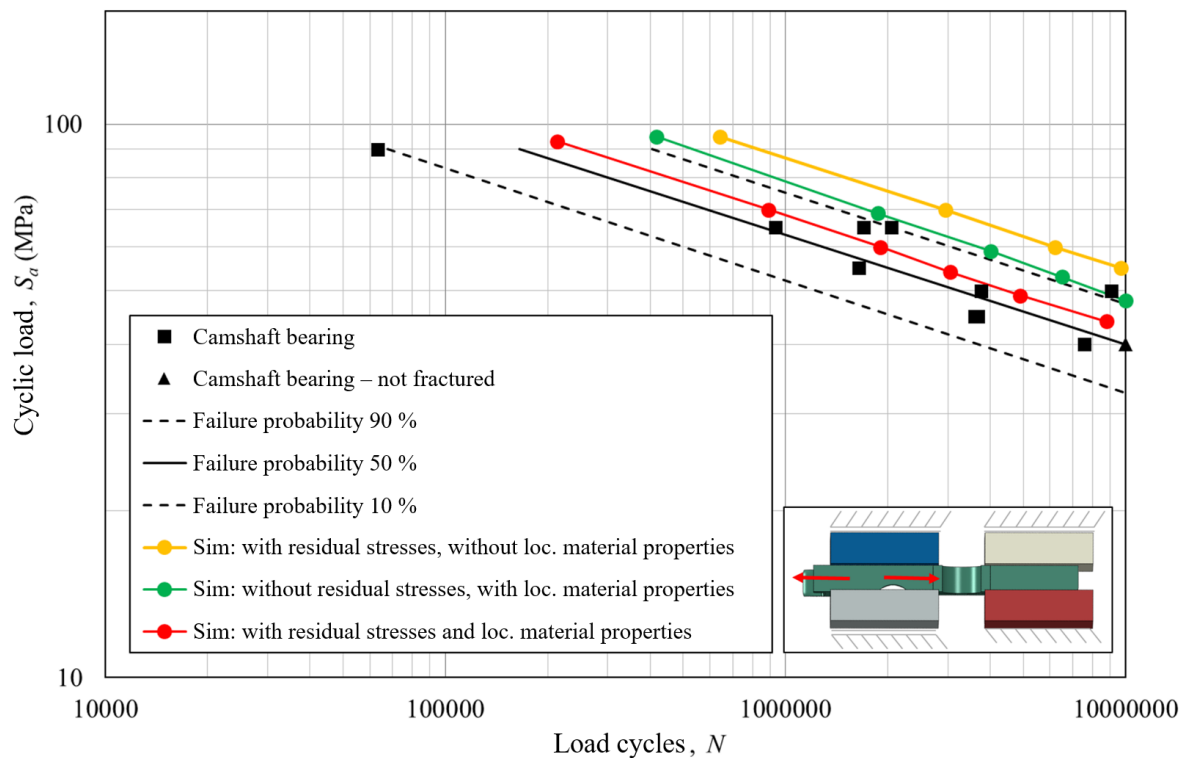*Figure 7: Presentation of the newly developed concept for predicting the actual failure behavior of aluminum castings*

Figure 8: Result of the tension-compressive fatigue test of the cylinder head camshaft bearing samples (R = -1) of the alloy AlSi7Cu0.5Mg (T6W) [13]

8. Summary and Conclusion

In the course of a comprehensive analysis of microporosity in cylinder heads for two typical casting alloys, a correlation between the characteristic pore size, pore shape, and the overall porosity of the samples was determined. In this process, the sphericity of the pores decreases

continuously, whereas the maximum pore dimensions increase with increasing porosity. Both dependencies are directly related to the mechanisms of pore formation in a dendritic microstructure, which determines both the pore shape and the pore size. The determined relationship was used to predict a porosity-based fatigue strength. In addition to the cooling rate, this allows both the local feeding properties and the specific solidification characteristics of the alloy to be taken into account; thus significantly improving the local prediction of the cyclic fatigue strength of the component. Furthermore, the residual stress state after T6W heat-treatment was considered. With the help of validation tests, it could be demonstrated that the local fatigue strength, as well as the residual stress state, are necessary to achieve a satisfactory accuracy in the prediction of the failure behavior. The developed methodology thus represents a significant extension of previously used methods for the design of highly loaded cast components. The targeted use of this approach in the context of virtual designs of experiments (DoE) promises a precise development of components as well as their robust production in the real casting process.

9. Acknowledgments

10. References

[1]   M. J. Couper, A. E. Neeson, und J. R. Griffiths, „Casting defects and the fatigue behaviour of an aluminium casting alloy", *Fatigue Fract. Eng. Mater. Struct.*, Bd. 13, Nr. 3, S. 213–227, 1990.

[2]   C. Garb, M. Leitner, und F. Grün, „Fatigue Strength Assessment of AlSi7Cu0.5Mg T6W Castings Supported by Computed Tomography Microporosity Analysis", *Procedia Eng.*, Bd. 160, S. 53–60, Jan. 2016.

[3]   H. Meishner und F. J. Feikus, „Gießverfahren zur Herstellung von Aluminium-Zylinderköpfen und -Zylinderkurbelgehäusen [Casting processes for aluminium cylinder head and crankcase production]", *Giesserei*, Bd. 102, S. 34–41, 2015.

[4]   C. Garb, M. Leitner, M. Tauscher, M. Weidt, und R. Brunner, „Statistical analysis of micropore size distributions in Al–Si castings evaluated by X-ray computed tomography", *Int. J. Mater. Res.*, Bd. 109, Nr. 10, S. 889–899, Aug. 2018.

[5]   M. Weidt und C. Thomser, „Methodische Integration der virtuellen gießtechnischen Optimierung in die Bauteilentwicklung zur betriebsfesten und robusten Auslegung von hochbelasteten Aluminiumgussteile", in *VDI-Berichte*, Magdeburg, Germany, 2019, Bd. 2339, S. 23–37.

[6]   G. Heiberg, K. Nogita, M. Raanes, A. L. Dons, A. K. Dahle, und L. Arnberg, „Effect of magnesium, iron and copper on eutectic solidification of hypoeutectic aluminum-silicon alloys", *AFS Trans.*, Bd. 110, S. 347–358, 2002.

[7]   S. D. McDonald, A. K. Dahle, J. A. Taylor, und D. H. StJohn, „Modification-related porosity formation in hypoeutectic aluminum-silicon alloys", *Metall. Mater. Trans. B*, Bd. 35, Nr. 6, S. 1097–1106, Dez. 2004.

[8]   C. M. Dinnis, J. A. Taylor, und A. K. Dahle, „Iron-related porosity in Al–Si–(Cu) foundry alloys", *Mater. Sci. Eng. A*, Bd. 425, Nr. 1–2, S. 286–296, Juni 2006.

[9]   C. Villeneuve, A. M. Samuel, F. H. Samuel, H. W. Doty, und S. Valtierra, „Role of trace elements in enhancing the performance of 319 aluminum foundry alloys", *AFS Trans.*, Bd. 109, S. 39–60, 2001.

[10] M. Weidt, R. A. Hardin, C. Garb, J. Rosc, R. Brunner, und C. Beckermann, „Prediction of porosity characteristics of aluminium castings based on X-ray CT measurements", *Int. J. Cast Met. Res.*, S. 1–19, Mai 2018.

[11] K. D. Carlson und C. Beckermann, „Prediction of Shrinkage Pore Volume Fraction Using a Dimensionless Niyama Criterion", *Metall. Mater. Trans. A*, Bd. 40, Nr. 1, S. 163–175, Jan. 2009.

[12] C. Garb, „Materialmodellentwicklung für die betriebsfeste Auslegung von Aluminiumgussbauteilen unter Berücksichtigung mikrostruktureller Größen", Dissertation, Montanuniversität Leoben, 2018.

[13] M. Smolnikar, M. DeJack, M. Strasek, R. Tichy, und K. Czubernat, „Impact of Material Behavior on Engine Development - Influence of Porosity on Fatigue Life in Aluminum (part II)", gehalten auf der Femfat User Conference, Steyr, Österreich, 2019.

[A]   MAGMASOFT® is a product of MAGMA Gießereitechnologie GmbH, Aachen.

      MAGMASOFT ® is an international trademark brand of MAGMA GmbH.

Captions

Figure 1: Representation of the largest dimension of a convex pore envelope (d_e)

Figure 2: Three-dimensional representation of an XCT sample from the tween deck of an AlSi8Cu3 cylinder head. The porosity is 0.176 %, the maximum diameter of the pore envelope is $d_{e,max}$ 2.75 mm. The coloring of the individual pores is done randomly and serves only for better differentiation of the individual pores [5].

Figure 3: Maximum envelope diameter plotted against porosity [5].

Figure 4: Volume-weighted mean sphericity versus porosity

Figure 5: Representation of the simulated Von Mises equivalent stress after T6W heat-treatment of the entire cylinder head (top left), in the camshaft bearing as part of the cylinder head (bottom left) and after mechanical extraction of the camshaft bearing for the validation tests (center)

Figure 6: Plot of the tension-compressive fatigue strength in section through the center of the camshaft bearing using the "classical" approach, based on the local DAS (left), as well as based on the additionally included microporosity prediction and the derived defect size (right)

Figure 7: Presentation of the newly developed concept for predicting the actual failure behavior of aluminum castings

Figure 8: Result of the tension-compressive fatigue test of the cylinder head camshaft bearing samples (R = -1) of the alloy AlSi7Cu0.5Mg (T6W) [13]